

SYNTHESIS AND CHARACTERIZATION OF TWO-
DIMENSIONAL TRANSITION METAL DICHALCOGENIDES

BY

ZIHAN YAO

THESIS

Submitted in partial fulfillment of the requirements
for the degree of Master of Science in Electrical and Computer Engineering
in the Graduate College of the
University of Illinois at Urbana-Champaign, 2017

Urbana, Illinois

Adviser:

Assistant Professor Wenjuan Zhu

Abstract

Semiconducting transition metal dichalcogenides (TMDCs) have attracted intense research interest in recent years, due to their many unique electrical, optical, and mechanical properties and their potential for diverse applications. One of the key challenges in 2D TMDC electronics is to synthesize high-quality and large-scale monolayer TMDCs.

In this thesis, I have systematically investigated the growth of MoS₂ and WSe₂ using chemical vapor deposition (CVD) and metal-organic chemical vapor deposition (MOCVD) methods. I studied the impact of the growth conditions, including temperature, pressure, gas flow rate, precursor type, precursor quantify, the position of the solid precursor, and seed layer dispersion, on the morphology of the MoS₂ and WSe₂ film. Optical imaging, Raman and photoluminescence (PL) spectroscopy, and atomic force microscopy (AFM) were used to measure the synthesized film. Electronic devices including transistors, Hall-bars and transmission line microstrips (TLMs) were fabricated. Current transport of these devices was measured at various temperatures. Based on the systematic investigation and process optimization, we were able to successfully grow monolayer WSe₂ with grain size up to 30 micrometers. At room temperature, the carrier mobility reaches 7.5 cm²/V-s. In addition, we have successfully grown MoS₂ using gas phase precursor H₂S and molybdenum hexacarbonyl (MHC) for the first time. These gas phase precursors can potentially enable wafer scale growth of TMDCs.

This study provides comprehensive information and in-depth understanding of the synthesis of WSe₂ and MoS₂ using CVD and MOCVD methods. The resulting monolayer WSe₂ and MoS₂ materials provide a solid material foundation for future study of the electronic and photonic devices based on these materials. These novel devices will have a broad range of applications in computing, communication, and biomedicine.

Acknowledgments

I would like to thank everyone who helped me during my master of science studies. Firstly, I sincerely thank my advisor, Professor Wenjuan Zhu, for all the support and help. Professor Zhu has provided me with many useful ideas and suggestions, and always guided me towards the right track throughout my master of science studies.

I would like to thank all current and previous Zhu group members for helping me out whenever I was in need: Jialun Liu, Zhengfeng Yang, Wuichung Yap, Sifan Wang, Yanda Hu, Haonan Wu, Mike Yang, Yongxin Li, Yueming Yan, Yunwen Zhou and Kai Xu.

Thank you to all the Micro and Nanotechnology Laboratory staff for training me on the tools and helping me out whenever I was in need.

I would like to thank my parents for their support and encouragement.

Finally, I would like to thank my fiancé for her endless love and support. I could not have finished my degree without her support.

Contents

1. Introduction.....	1
1.1 Monolayer MoS ₂ by metal-organic chemical vapor deposition (MOCVD)	1
1.2 Monolayer WSe ₂ by chemical vapor deposition (CVD)	1
2. Literature Review.....	3
2.1 Role of the seeding promoter in monolayer MoS ₂ synthesis.....	3
2.2 Growth mechanism study on WSe ₂	3
3. Description of Research Results	5
3.1 Morphology changes of MoS ₂ by CVD with flow rate of argon (Ar) and growth time	5
3.2 Monolayer MoS ₂ growth by MOCVD.....	8
3.2.1 Experiment setup.....	8
3.2.2 Result of growth by MOCVD and discussion.....	9
3.2.3 Raman spectroscopy and photoluminescence spectroscopy of MoS ₂	11
3.2.4 Comparison between CVD and MOCVD, solid precursor and gas precursor	12
3.3 Monolayer WSe ₂ growth and electrical characterization.....	13
3.3.1 Growth setup and general operation procedure	13
3.3.2 Differences in CVD between MTI and TMD furnace	14
3.3.3 Approach toward monolayer WSe ₂ growth	14
3.3.4 Optimized recipe and results	20
3.3.5 Raman spectroscopy and photoluminescence spectroscopy of WSe ₂	21
3.4 WSe ₂ device fabrication.....	23
4. Conclusion	28
References.....	29
Appendix: Optimized MoS ₂ by CVD Operation Procedure.....	31

1. Introduction

1.1 Monolayer MoS₂ by metal-organic chemical vapor deposition (MOCVD)

Metal-organic chemical vapor deposition (MOCVD) is a method to realize ultra-thin films deposition [1]. Previously, MOCVD was applied to various types of growth of semiconductor material. It is widely applied because of the comparatively excellent quality of material synthesized from MOCVD. Recently, the monolayer of MoS₂ grown from molybdenum hexacarbonyl (MHC) and diethyl sulphide (DES) by MOCVD has been verified with excellent electronic properties and availability for wafer-scale coverage [2]. Thus, it is exciting to figure out the method for the monolayer MoS₂ deposition with organic precursor, molybdenum hexacarbonyl (MHC) and hydrogen sulfide. In section 3.2, a unique method will be reported together with optical readout of the flake obtained.

1.2 Monolayer WSe₂ by chemical vapor deposition (CVD)

Semiconducting transition metal dichalcogenides (TMDCs) have attracted a lot of attention recently because of their interesting electronic, optical, and mechanical properties. Among large numbers of TMDCs, monolayer tungsten diselenide (WSe₂) is of particular interest since it possesses a direct band gap and tunable charge transport behaviors, which make it suitable for a variety of electronic and optoelectronic applications [3-5]. Direct synthesis of large domains of monolayer WSe₂ and their growth mechanism studies are important steps toward applications of WSe₂. Here, we report systematic studies on ambient pressure chemical vapor deposition (CVD) growth of monolayer and few-layer WSe₂ flakes directly on silica substrates. The WSe₂ flakes were characterized using optical microscope and Raman spectroscopy, and photoluminescence spectroscopy. We investigated how growth parameters, with emphases on growth temperatures

and durations, affect the sizes, layer numbers, and shapes of as-grown WSe₂ flakes. We also demonstrated that transport properties of CVD-grown monolayer WSe₂, similar to mechanically exfoliated samples, can be tuned to either p-type or ambipolar electrical behavior, depending on the types of metal contacts. These results deepen our understanding of the vapor phase growth mechanism of WSe₂, and may benefit the uses of these CVD-grown monolayer materials in electronics and optoelectronics.

2. Literature Review

2.1 Role of the seeding promoter in monolayer MoS₂ synthesis

Ling et al. [6] is the first study of the growth of MoS₂ and WSe₂. The study investigates the effects of different seeding promoters and the seed concentration. It also comprehensively and systematically illustrates the promotion by seeds and introduces its diffusion effect, providing many useful ideas for our research.

Photoluminescence (PL) and Raman spectroscopy indicate that by using perylene-3, 4, 9, 10-tetracarboxylic acid tetra potassium (PTAS) seeding promoter, MoS₂ monolayer can be obtained easily. Without the promotion of seeding promoters, weaker intensity of PL was observed. The comparison between two cases was illustrated.

The diffusion effect was illustrated by using a promoter substrate placed upstream. The monolayer MoS₂ grew in the regions away from the seeding pattern, and there was a gradient dependence between nucleation density and distance from the promoter substrate.

The comprehensive investigation collected the information from the growth using different aromatic molecules including organic and inorganic seeding promoters. The PTAS delivered the best result, promoting larger coverage and excellent quality of MoS₂.

2.2 Growth mechanism study on WSe₂

Liu et al. [7] introduce a method for WSe₂ monolayer deposition on Si/SiO₂ substrate.

They first note the defects in the as-grown WSe₂ by providing the Raman data and suggest insufficiency of Se may lead to defects during the formation of WSe₂. Also, the different

termination with W or Se atom may lead to different morphology. Here the outward curved edges and hexagon deposition were observed.

Secondly, they discuss the influence of growth parameters such as temperature and growth time. The morphology change at different temperatures and different durations was observed. The growth temperature and growth duration have significant effects on the sizes, layer numbers and shapes of WSe₂ flakes, providing the approach to obtain the larger grains with high quality. The results were verified with optical images and photospectroscopy data.

Liu et al. provide the motivation for my project aimed at optimizing WSe₂ growth according to growth condition.

3. Description of Research Results

3.1 Morphology changes of MoS₂ by CVD with flow rate of argon (Ar) and growth time

A three-zone MTI furnace was used for MoS₂ growth by CVD. For the MoS₂ growth by CVD, the flow rate of Ar and growth time are the key effects on the morphology of MoS₂. The different combinations of Ar flow rate and growth time lead to different morphologies of MoS₂ deposition. From observation and validation, the increase of growth time can lead the crystal to extend horizontally and increase in size; and flow rate of Ar in sccm (standard cubic centimeter per minute), with varying the concentration and partial pressure of Ar, leads to increased nucleation density, stack of layers and thick layers. The detailed operation setup is provided in the Appendix and it is similar to the procedure for WSe₂ growth.

The temperature programming process of growth is illustrated in Figure 1.

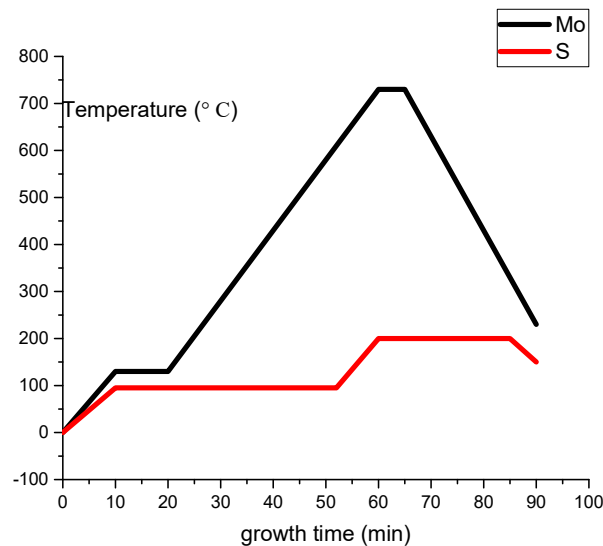


Figure 1 The temperature programming process of growth

The trial was taken in four different conditions. The morphologies in each case are summarized in Table 1. The morphology changes at different temperatures and different Ar flow are clear.

Table 1 Morphology changes under different flow rates of Ar and growth time

<div> <div>flow rate of Ar (sccm)</div> <div>Time (min)</div> </div>	15	400
10	Small grains, smaller than 5 μm in size	Small grains merge into continuous layer, separate grains appeared to be larger
30	At the edge of substrate, multilayered flakes emerged from the edge of crystal	Continuous layer formed, and stacked layer onto continuous layer

From comparison of the set of optical images (Figure 2), triangular crystals extend horizontally when growth duration increases from 10 min to 30 min.

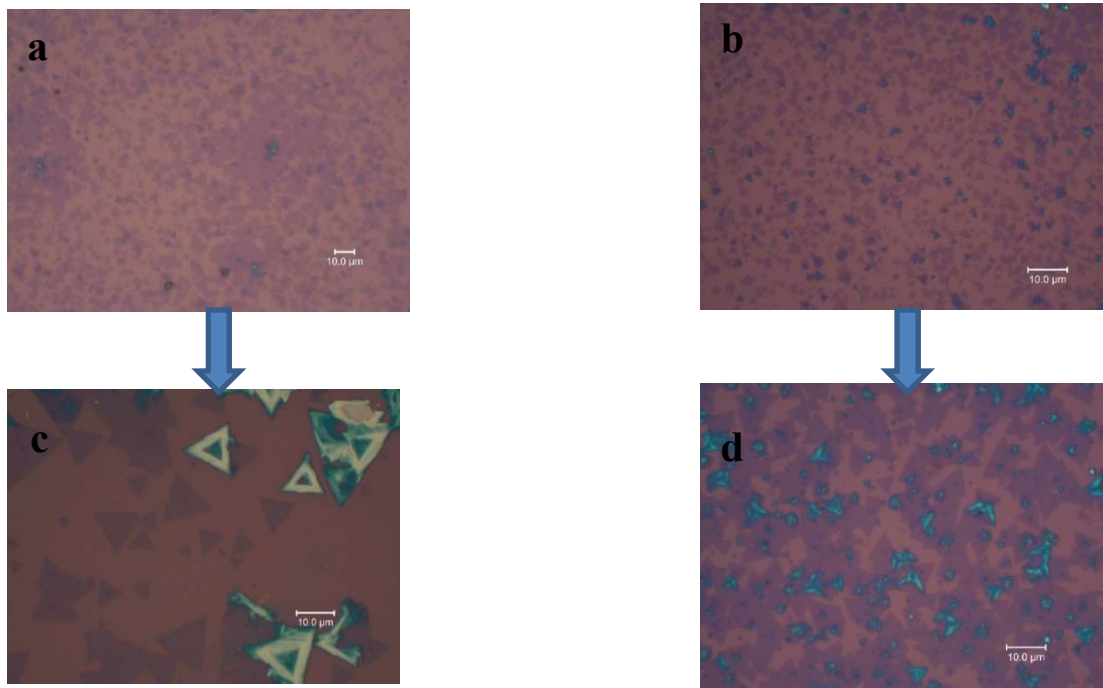


Figure 2 Horizontal extension trend from increase of growth time. (a) 10 min, 15 sccm Ar. (b) 10min, 400 sccm Ar. (c) 30 min, 15 sccm Ar. (d) 30 min, 400 sccm Ar.

From comparison of the set of optical images (Figure 3), we observe that crystals start to stack vertically when growth duration increases from 10 min to 30 min, and single crystals merge into a continuous layer with huge increase of nucleation density when Ar flow increases from 15 sccm to 400 sccm.

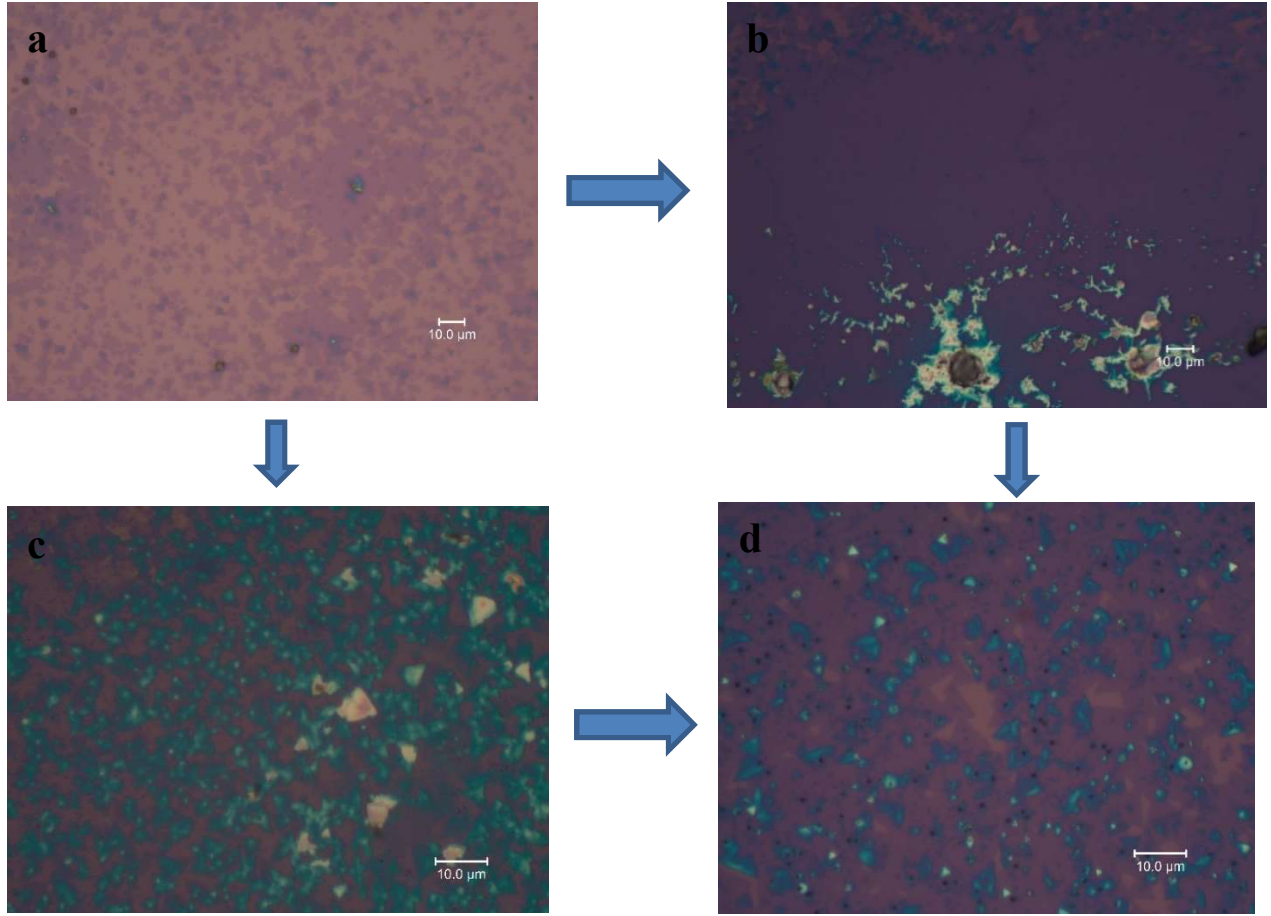


Figure 3 Vertical and horizontal extension trend from increase of growth time and increase of Ar. (a) 10 min, 15 sccm Ar. (b) 10 min, 400 sccm Ar. (c) 30 min, 15 sccm Ar. (d) 30 min, 400 sccm Ar.

As can be seen from the optical images of sample in each case, the extreme condition of 400 sccm Ar for 30 min provides the clear crystal growth horizontally and vertically. The investigation of morphology sensitivity to the temperature and Ar flow helps to find the way to grow monolayer WSe₂, which will be discussed in the next chapter. The reported trend might be

not too similar to the growth mechanism in MOCVD, but the approach did provide the idea for the improvement of the formation of crystals during MOCVD.

3.2 Monolayer MoS₂ growth by MOCVD

3.2.1 Experiment setup

A three-zone MOCVD furnace was used to perform the synthesis of monolayer MoS₂. The growth was conducted in vacuum pressure between 4 and 8 Torr. The growth temperature was 600 °C and growth time was 300 min. The flow rates of precursors were 50 sccm for Ar, 0.5 sccm for H₂, 0.2 sccm for molybdenum hexacarbonyl (MHC) and 4 sccm for H₂S. The Si/SiO₂ substrate with 285 nm SiO₂ was used for the growth and prepared by piranha cleaning (detailed cleaning procedure is introduced in the Appendix).

Typically, the sliced wafer was vertically placed in the wafer boat to increase the contact area between the substrate and precursor. Thus, the greater contact promotes the deposition of MoS₂. The boat was loaded into the center zone.

The temperatures of the three furnace zones were set to be the same. The growth temperature was ramped up as follows: initially, the temperature was ramped at 10 °C/min to 120 °C and held for 20 min to evaporate water residue inside the tube. Then, temperature was ramped at 15 °C/min to 600 °C and held at this temperature for the growth.

3.2.2 Result of growth by MOCVD and discussion



Figure 4 Optical image of the first-time flake deposition

The first-time monolayer deposition (Figure 4) was achieved with the flow of 0.3 sccm MHC, 9 sccm H_2S , 0.5 sccm H_2 and 50 sccm Ar and 300 min duration. The trial shows reproducibility and the product has large deposition but not completely triangular crystals from bottom to center of the substrate. The size of crystals decreases gradually from bottom to center. The size of triangles at the bottom of the substrate is around 5-10 μm and it becomes less than 1 μm at the center of the substrate. The deposition has been verified to be monolayer MoS_2 but it has limited optical quality.

According to the optical image of the sample, the triangle crystals are uncompleted and the edges of triangles are curved inward. The previous study on the synthesis of monolayer MoS_2 provided the explanation for the inward curved edges and small dimensions [6]. It suggested that flow of Ar and growth duration greatly affect the size and shape of crystals. Thus, another trial was taken by decreasing the flow rate of Ar from 50 sccm to 25 sccm and increasing the growth duration from 300 min to 540 min. The optical result in Figure 5 shows that the nucleation density increases and the coverage of triangle crystals extends to most of the bottom (Figure 5).

Compared to the previous product with 50 sccm flow of Ar and 300 min growth duration which has very little deposition in the middle of the substrate, the noticeable deposition extends the coverage to the middle of the substrate and appears as small grains (Figure 6).

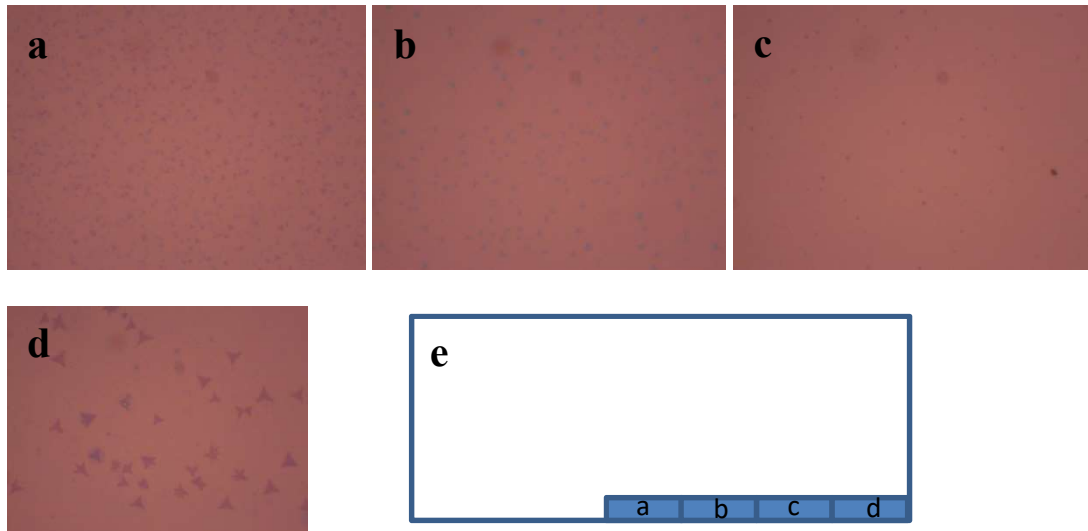


Figure 5 Morphology trend from bottom-center to bottom-right. (a) Bottom center, (b) bottom center toward bottom right, (c) bottom toward bottom right further, (d) bottom right corner and, (e) correlated positions looked at from top with respect to (a), (b), (c) and (d).

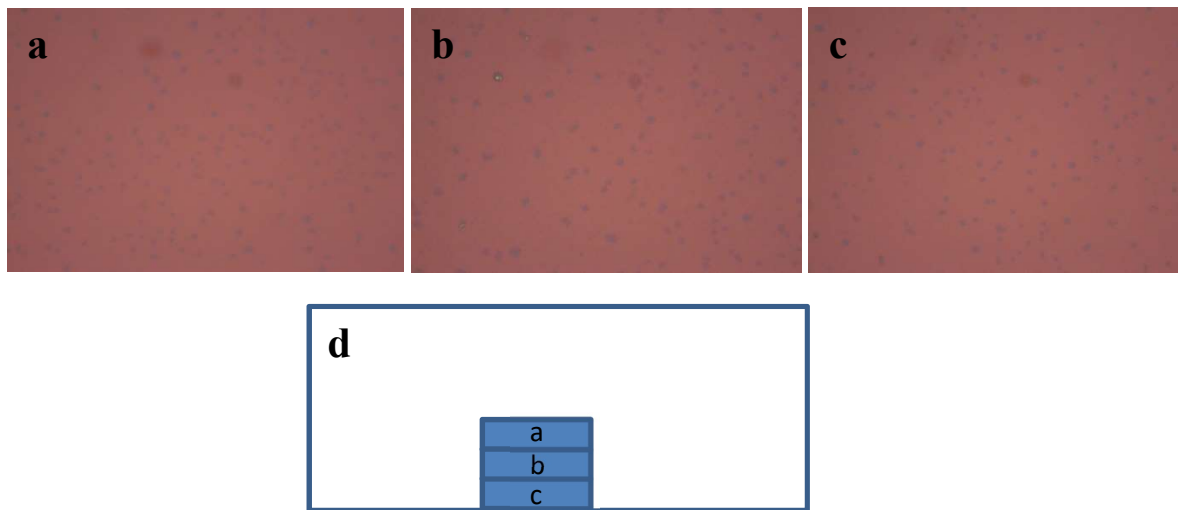


Figure 6 Morphology trend from bottom to center. (a) Center, (b) center toward bottom, (c) bottom, and (d) correlated position looked at from top with respect to (a), (b) and (c).

3.2.3 Raman spectroscopy and photoluminescence spectroscopy of MoS₂

Raman and PL spectra confirm the quality of the material grown. Raman and PL are consistent with previous reports for single layer MoS₂. The spacing between A_{1g} peak and E_{2g} peak is approximately 19 cm⁻¹ (Figure 7). PL spectrum has high intensity at 1.86 eV, consistent with the single layer direct bandgap of MoS₂ at 1.8 eV [8-10]. Both A and B excitons are noticeable (Figure 8).

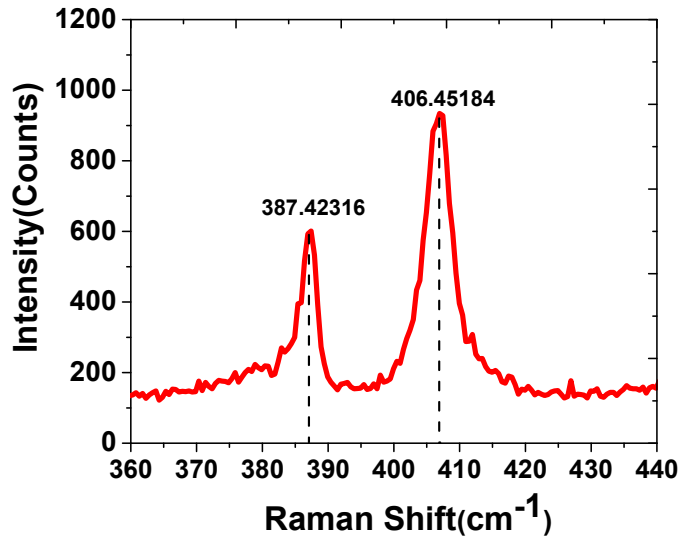


Figure 7 Raman spectroscopy of monolayer MoS₂

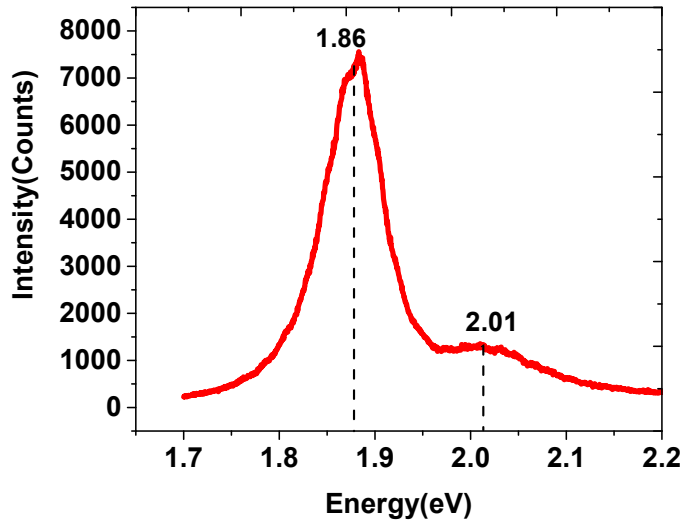


Figure 8 Photoluminescence spectroscopy of MoS₂

3.2.4 Comparison between CVD and MOCVD, solid precursor and gas precursor

Normally, the quantity of solid precursor supplied to CVD is very hard to control precisely. The vaporization of sulfur precursor greatly relies on the preset zone temperature. Thus, it is hard to quantify how much the solid precursor is vaporized and supplied to the growth period. In comparison, MOCVD can realize the constant supply of gas precursor or solid precursor by setting the flow rate of each in the control panel.

Despite PTAS having demonstrated its ability to enhance Raman spectrum intensity [6], it will bring many restrictions to the processing in the next steps. For instance, the piranha cleaned substrate with PTAS cannot involve the use of water during processing. In contrast, the single crystals or even continuous monolayer with high quality can be achieved by MOCVD without PTAS [6]. It has been partially verified by previous trials because monolayer MoS₂ has been

grown without PTAS, but the growth product still needs further improvement in quality, morphology and distribution.

Besides the difference reported above, other basic differences are summarized in Table 2.

Table 2 Comparison between solid precursor and gas precursor

	H ₂ S	S powder
Pressure (Torr)	1-10	760
Growth time (min)	300-720	5-30
Grain size (μm)	5-10	20
Distribution	Uniform in nucleation density	Uniformity depend on PTAS

3.3 Monolayer WSe₂ growth and electrical characterization

3.3.1 Growth setup and general operation procedure

One zone furnace was used for CVD growth of WSe₂. The schematic of our CVD setup is shown in Figure 9. Specifically, Se powders (300 mg, 99.5%, Sigma-Aldrich) were placed in the edge of the zone at upstream, and WO₃ powders (150 mg, 99.9%, Sigma-Aldrich) were placed in the left side of the center of the zone. The distance between the two sources was tuned and optimized at approximately 20 cm. If the Se is too close to the WO₃ holder, the distribution of Se flow over the WO₃ will lead to nonuniform deposition. A 2-inch quartz reaction tube was firstly flushed with 100 sccm Ar for 30 min, and then the furnace was ramped to the designed temperature at a ramp rate of 30 °C/min. The temperature of WO₃ was optimized at 875 °C and growth time can be varied from 5 min to 15 min or even longer. The growth substrates were silicon wafers with

285 nm SiO₂, which were placed face down on top of the WO₃ powders. During the growth, the flow rate of Ar/H₂ was optimized at 70/20 sccm, and the growth was taken at ambient pressure. After reaction, the furnace naturally cooled down to below 200 °C under 20 sccm Ar, and then the sample would be ready to remove for electrical characterization.

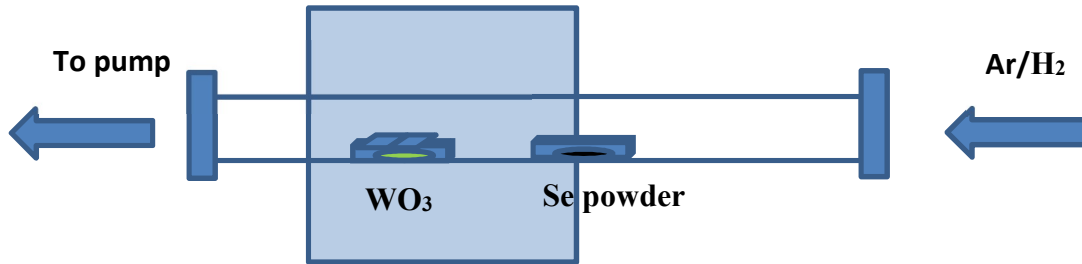


Figure 9 Schematic of TMD CVD setup

3.3.2 Differences in CVD between MTI and TMD furnace

There are three major differences between MTI and TMD furnace during growth:

1. The TMD furnace has only one zone. It needs manually adjustment of the vapor temperature of Se by changing the position of WO₃ powder and boat.
2. The use of reductive species like H₂ or sulfur will facilitate sublimation of WO_{3-x} to increase its concentration in vapor phase [11,12] and thus promote WSe₂ growth.
3. Physical dimensions of MTI furnace and TMD furnace are greatly different, necessitating separate consideration of the flow rate of Ar applied to growth.

3.3.3 Approach toward monolayer WSe₂ growth

To achieve the monolayer WSe₂ deposition, several growth parameters must be considered, including pressure, flow rate of H₂, amount and location of precursor and amount of PTAS coating. The general approach was to start with the parameters from previous reports [7] and

adjust each parameter by the analysis of experiment data and results. Following are experiment results and discussion of each growth parameter.

1. Change growth temperature

Some thick crystals were first found at 975 °C. Since WO_3 will be more volatile at high temperature, more WO_{3-x} will vaporize and form thick layers. Thus, decrease in temperature is supposed to be an approach to grow few-layer crystals.

As expected, the experiments done at 925 °C and 875 °C show a morphology change from multilayer and thick crystals to monolayer crystals (Figure 10).

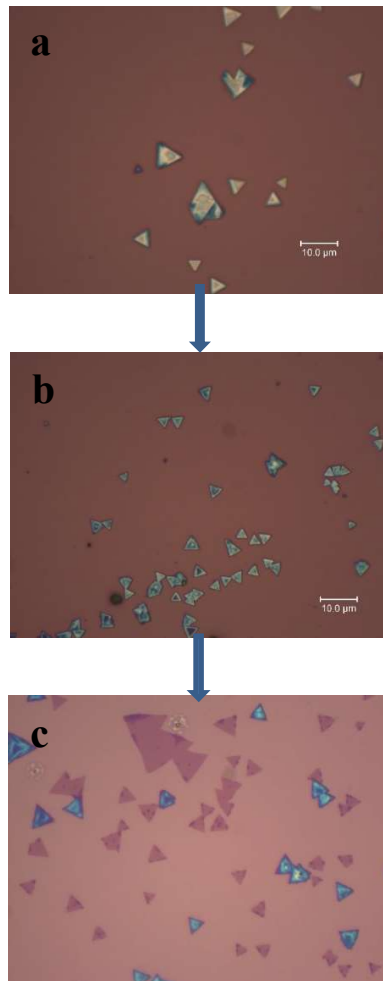


Figure 10 Optical images at different temperature. (a) 975 °C, (b) 925 °C, and (c) 875 °C.

2. Quantity of WO_3

In the last section, monolayer deposition was obtained at 875 °C with 50/15 sccm flow of Ar/H₂. Thus, further work primarily focused on other growth parameters.

The quantity of WO_3 also affects the morphology of deposition. Increasing the quantity of WO_3 causes multilayer flakes to stack on monolayer flakes. As the amount of WO_3 was increased from 100 mg to 200 mg, the edges of crystals started to form thick layers while the area between the center and edges of crystals was still monolayer (Figure 11). In addition, bilayer and thick layers appeared again. If the quantity is continuously increased while keeping the other parameters the same, more thick layers will appear.

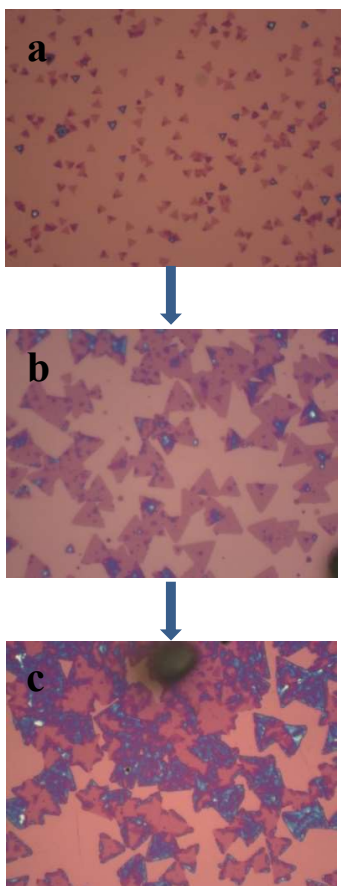


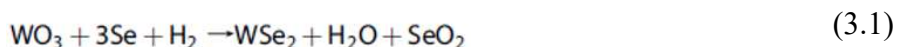
Figure 11 Optical images of samples grown with different quantities of WO_3 . (a) 100 mg, (b) 150 mg, and (c) 200 mg.

3. Pressure

Several trials were made under low pressure by connecting the furnace to a vacuum pump. However, the products had very little deposition on the substrate; grains were small, presumably due to reduced concentrations of reactants at low pressure. Then the general approach switched to growing under ambient pressure. The morphology started to change, with thick and small crystals deposited at 975 °C.

4. Hydrogen

It has been confirmed with several trials that no flake will be deposited onto substrate without H₂. These trials verify previous thermodynamic calculations showing that the selenization reaction of WO₃ is only possible with the presence of hydrogen [11-13]. The chemical reaction occurring during the selenization of WO₃ is as follows:



The quantity of hydrogen for the growth greatly affects the size and number of layers deposited on the substrate. On the one hand, if the flow of H₂ is too high, the reduction of WO₃ to W proceeds very efficiently. The rate of WO_{3-x} evaporation becomes slower and leads to the formation of small monolayer crystals (Figure 12). On the other hand, if the flow rate of H₂ is too low, the reduction from WO₃ to WO_{3-x} will be inefficient, and lead to little deposition (Figure 12).

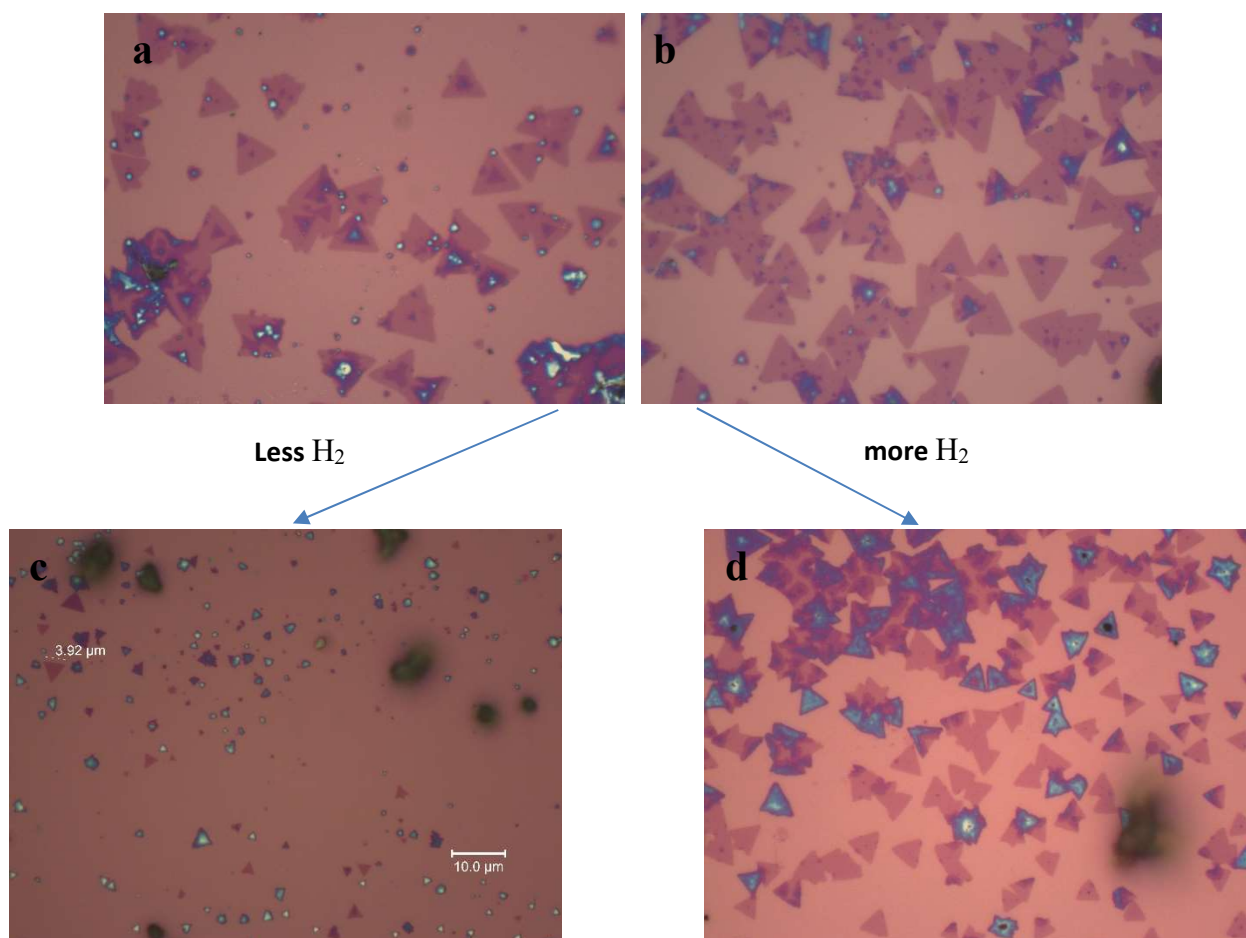


Figure 12 Optical images of samples grown with different flow rates of H₂. (a) and (b) 20 sccm, (c) 15 sccm, and (d) 25 sccm.

5. The ratio of flow rate between Ar and H₂

The Ar/H₂ ratios tried were from 4:1, 10:3, 3:1, and 12:5. The trend was not clear from comparison of optical images in each case. However, the nucleation density was observed to increase with increased concentration of H₂. Additionally, increased presence of H₂ would initiate the multilayer deposition, which appeared as big purple dots on the monolayer and incomplete bilayer.

6. The flow rate of Ar applied to growth

Increasing the flow rate of Ar while keeping the same ratio between Ar and H₂ will increase the local nucleation density while sacrificing the grain size (Figure 13). If the flow rate of Ar was increased to 80 sccm while keeping the flow rate of H₂ at 20 sccm, the nucleation density still increased. Small grains and thick crystals covered the entire substrate.

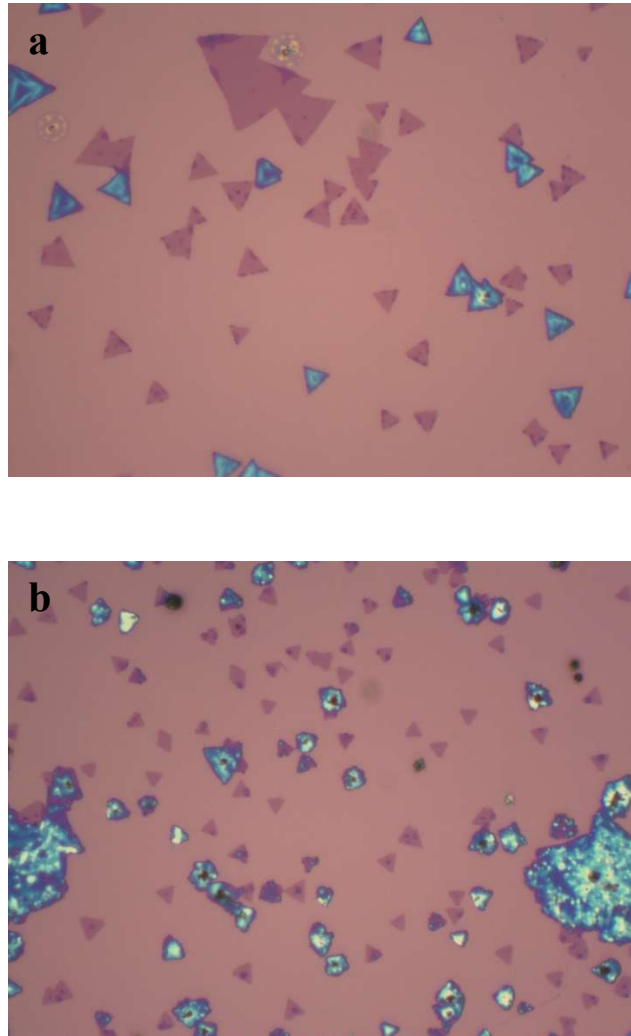


Figure 13 Optical images of samples grown with different flow rates of Ar. (a) 60 sccm, and (b) 75 sccm.

7. The distance between the boats with precursor

The distance between the boats with WO_3 and H_2 was optimized at 15-20 cm. If the boat with Se is too close to the boat with WO_3 , the distribution of Se vapor is nonuniform over the growth substrate and distribution of deposition is random and nonuniform.

3.3.4 Optimized recipe and results

Further optimization of the recipe was made according to previous optical images and observations. Large scale of monolayer deposition first appeared at 875 °C with 5 min duration and with 60/20 sccm flow of Ar/ H_2 . If 875 °C was regarded as a reference, samples grown at higher temperature such as 925 °C and 975 °C were smaller, with thicker layers and higher nucleation density. Flakes grown at lower temperature such as 850 °C were smaller but monolayer. The quantity of WO_3 also needs to be kept at the appropriate balance. Keeping Se constantly supplied to the growth, the flakes grown with more WO_3 normally were thicker. If flow rate of H_2 was considered as a reference, both higher and lower flow rates would lead to undesired morphology because the reduction of WO_3 was either too fast or too slow. If flow rate of Ar was regarded as a reference, the higher flow rate Ar would significantly increase the nucleation rate and provide more uniform distribution. The sample grown with 60 sccm flow of Ar only showed large monolayer crystals at the edge of the substrate, and much smaller crystals at the center. When the flow rate was increased to 70 sccm, better uniformity and better crystal morphology were achieved. Even continuous monolayer emerged in this case. Then, a reproducibility check was made to verify the applied growth recipe (Figure 14). The growth was finally optimized with the following conditions: ambient growth pressure, growth temperature at 875 °C, growth duration of 10 -15 min, 150 mg and 300 mg of WO_3 and Se, and 70/20 sccm flow of Ar/ H_2 .

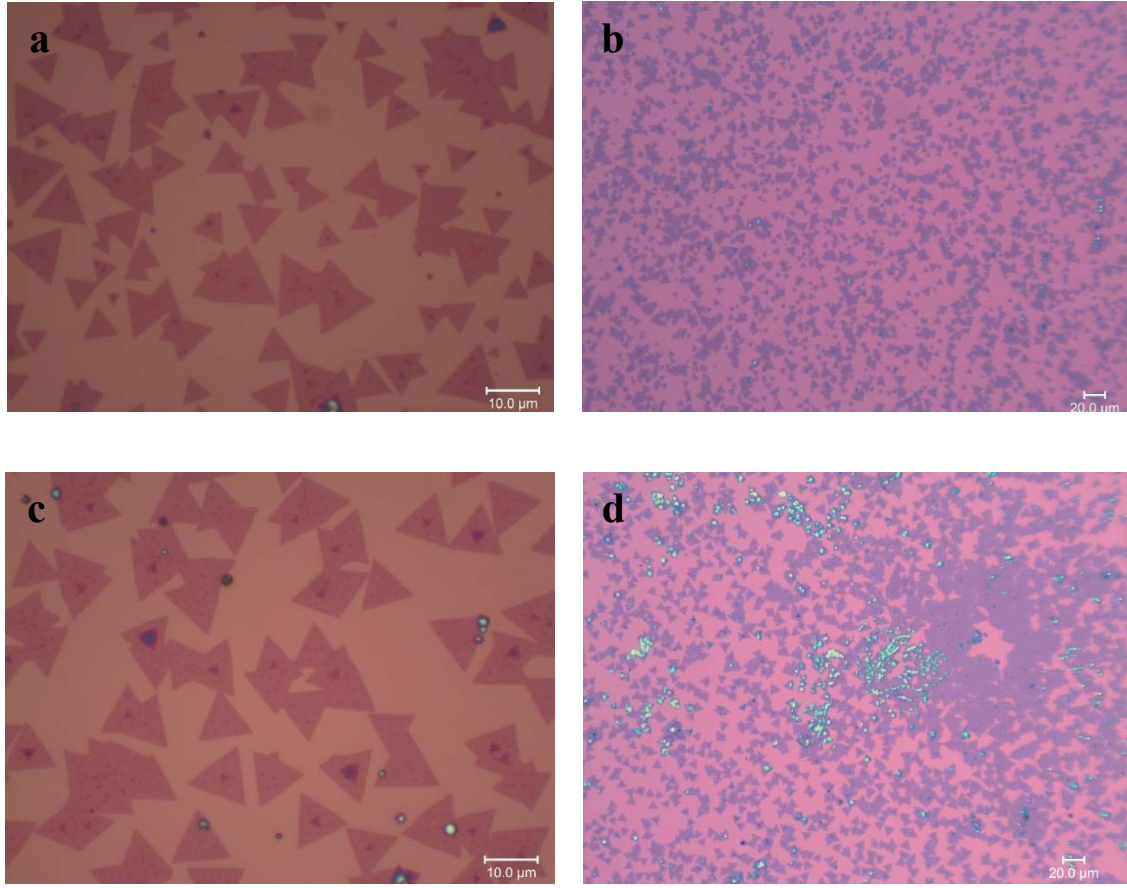


Figure 14 Optical images under 100x and 20x microscope collected from optimized recipe and trial for reproducibility. (a) and (b) First time optimization, and (c) and (d) double-check for reproducibility.

3.3.5 Raman spectroscopy and photoluminescence spectroscopy of WSe₂

For Raman and PL measurement, we used 532 nm laser with D2 energy level for 60 sec acquisition. Figure 15 shows that the A_{1g} and E_{2g} peaks are at 253 cm^{-1} and 263 cm^{-1} . Figure 16 shows a 0.2 eV wide PL peak at 1.6 eV. It shows the flake is monolayer with good quality and consistent with previous reports about Raman and PL of monolayer WSe₂ [11, 14].

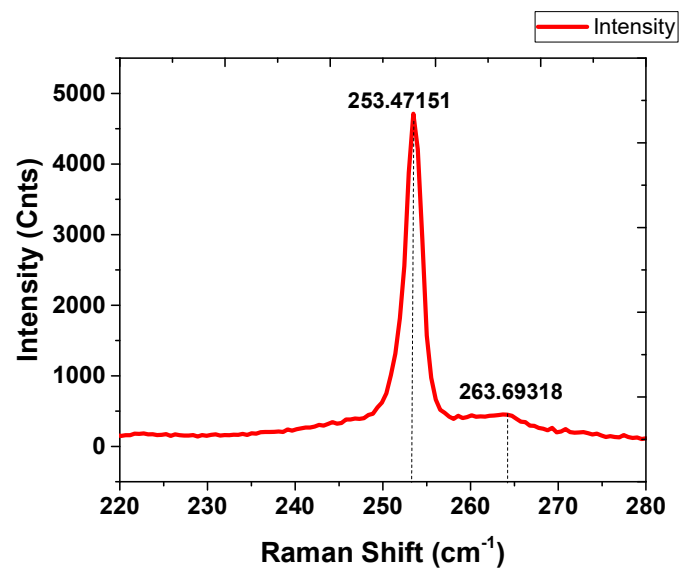


Figure 15 Raman collected from monolayer WSe₂ flake

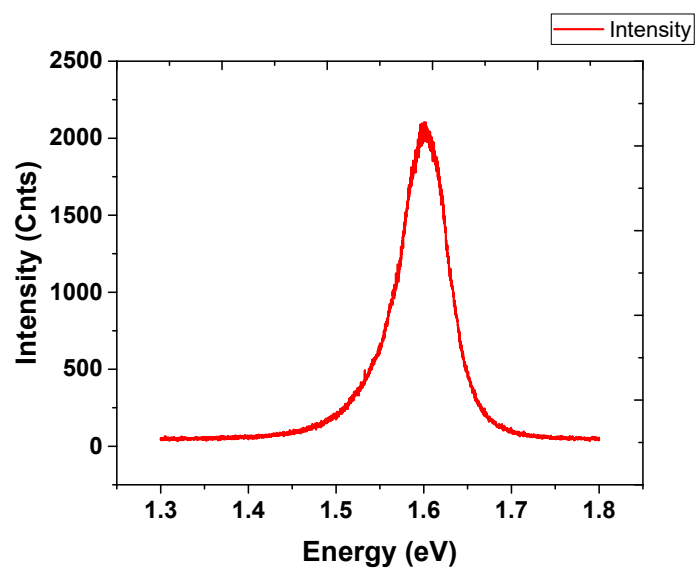


Figure 16 PL collected from monolayer WSe₂ flake

3.4 WSe₂ device fabrication

To investigate the electronic property of as-grown WSe₂, we directly fabricated back-gated WSe₂ FETs on as-grown WSe₂ monolayers.

The general fabrication process can be summarized as follows: The alignment mark was first defined on the substrate by e-beam lithography. Then we used e-beam evaporation to deposit Ti/Au with 5 nm/40 nm thickness on the pattern defined by the last step as an alignment mark. The devices were fabricated by repeating the same procedure used to create the alignment mark. Ti/Au (5 nm/50 nm) was used for the metal contact of the device. The device measurements were conducted in room temperature first, and then in low temperature.

Next, device measurements were conducted with variation of electronic parameters, primarily including I_d - V_g curve with variation of V_d (Figure 17), I_d - V_d curve with variation of V_g (Figure 18) and I_d - V_g curve with variation of temperature (Figure 19). According to the I_d - V_g and I_d - V_d curves, the device has strong field-effect signal and turn-on and turn-off properties with applied gate voltage. Also, applied with high back-gate voltages, the device behaves as a resistor because I_d increases linearly with increasing V_d . According to the I_d - V_g curve with variation of temperature, we see that I_d decreases as temperature decreases and shows a strong dependence on the temperature. This dependence is expected because the mobility and mobile carriers change with temperature.

Contact resistance, R_c , is calculated using following equation:

$$R_c = 0.5(R_{4pt} - R_{2pt} \times 2.5) \quad (3.2)$$

where R_{4pt} is the resistance between two sensing terminals in a Hall-bar structure measured by the four-point resistance method, while R_{2pt} is the measured two-point resistance between

source and drain in the Hall-bar device. The four-point resistance, two-point resistance and extracted contact resistance are shown in Figure. 20. We can see that contact resistance is comparable to the four-point channel resistance, indicating contact resistance plays a significant role in these devices.

The field-effect mobility is extracted from I_d - V_g curves using the following equation:

$$\mu_{FE} = \frac{I_D g_m L}{W V_D C_i} \quad (3.3)$$

where I_d is the source to drain current, and g_m is the partial derivative of I_d with respect to back-gate voltage. The extracted mobilities at various temperatures are shown in Figure 21(a) and the extracted mobilities at various back-gate voltages are shown in Figure 21(b). The mobility extracted from the two-point resistance increases dramatically with temperature, while the mobility extracted from four-point-resistance is nearly temperature independent (Figure 22). This can be explained by the influence of contact resistance on the mobility extraction. For two-terminal devices, the contact resistance decreases as the temperature increases, which gives higher extracted mobility. For four-point resistance measurement, however, since contact resistance has been eliminated by measurement, the temperature dependence of the extracted mobility reflects the true temperature dependence of carrier scattering. This weak temperature dependence is probably due to short-range scattering in WSe_2 .

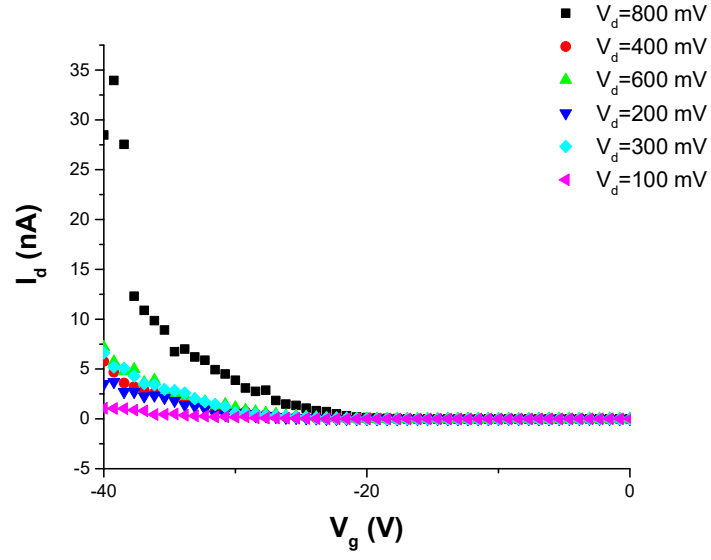


Figure 17 I_d - V_g curve with variation of V_d from 100 mV to 800 mV

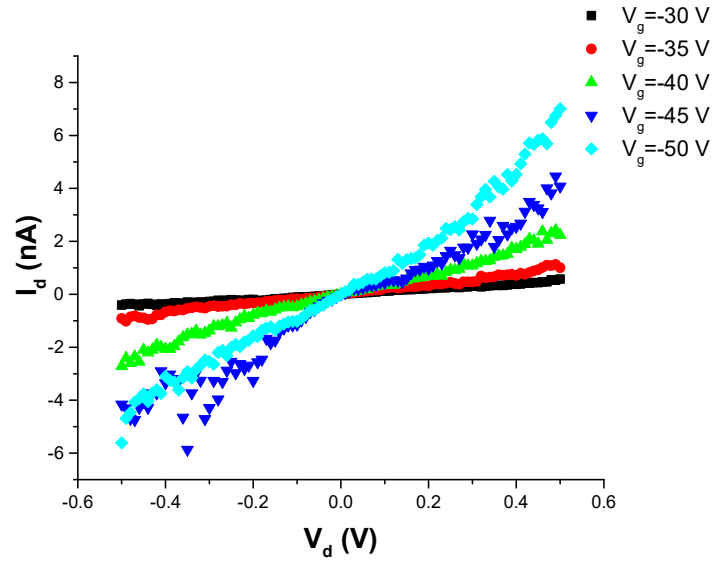


Figure 18 I_d - V_d curve with variation of V_g from -50 V to -30 V with a step of 5 V

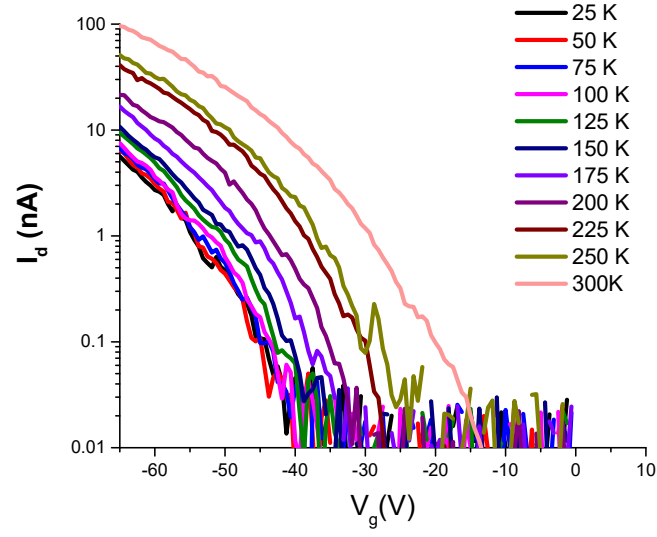


Figure 19 I_d - V_g with variation of temperature from 25 K to 300 K with a step of 25 K and fixed V_d at 1 V (device dimensions: $W = 3 \mu\text{m}$, $L = 0.5 \mu\text{m}$)

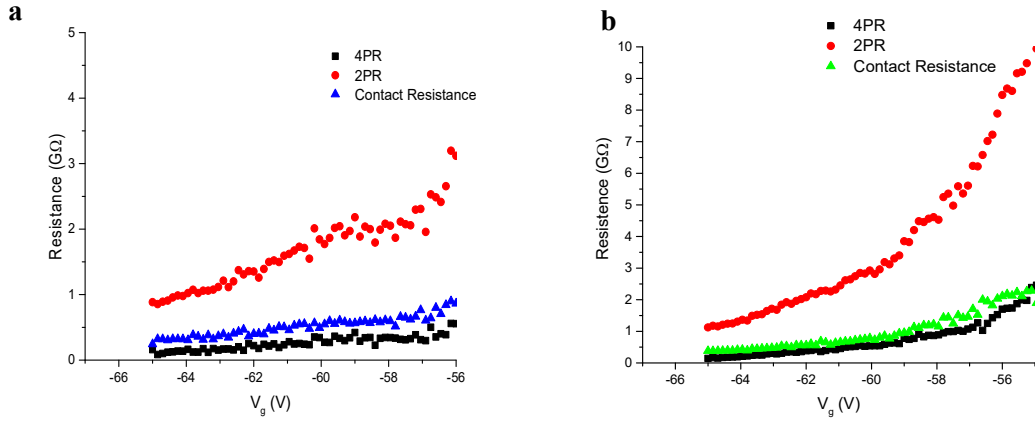


Figure 20 Contact resistance with variation of temperature. (a) 50 K and (b) 5 K. (Device dimensions: $W = 0.5 \mu\text{m}$, $L = 5 \mu\text{m}$, distance between sensing terminals = $2 \mu\text{m}$.)

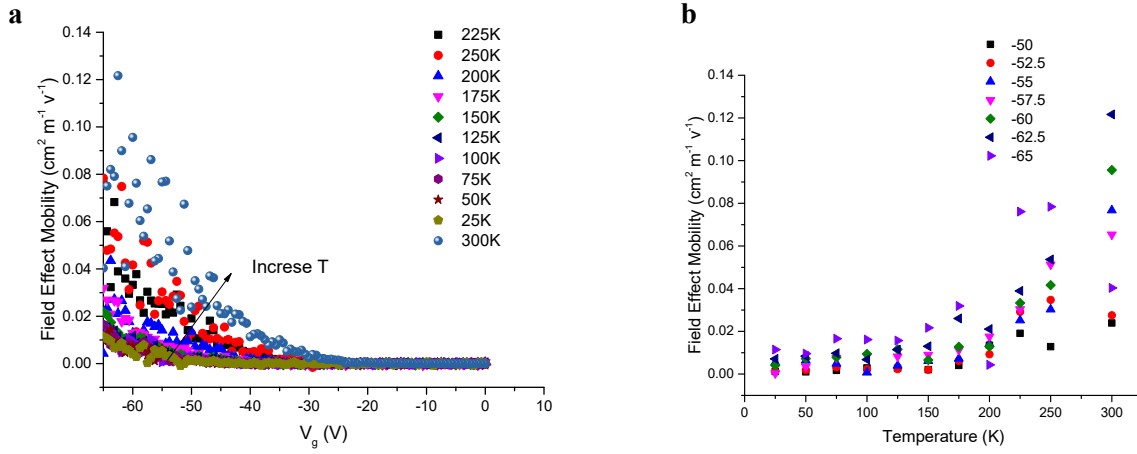


Figure 21 Field-effect mobility with different dependence. (a) Field-effect mobility versus V_g with variation of temperature and (b) field-effect mobility versus temperature with variation of gate voltage (device dimensions: $W = 3 \mu\text{m}$, $L = 0.5 \mu\text{m}$)

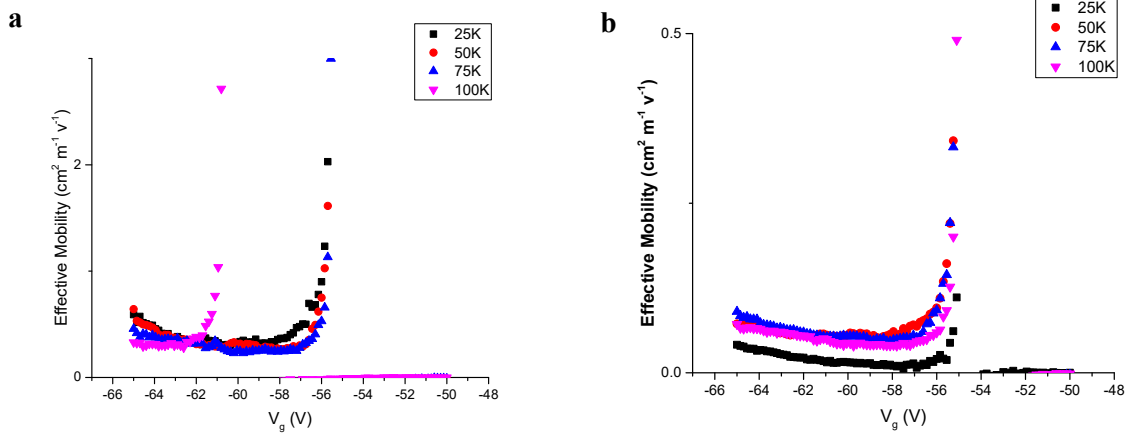


Figure 22 Effective mobility with variation of temperature extracted from (a) four-point-resistance and (b) two-point-resistance. (Device dimensions: $W = 0.5 \mu\text{m}$, $L = 5 \mu\text{m}$, distance between sensing terminals = $2 \mu\text{m}$.)

4. Conclusion

Uniformly distributed monolayer WSe₂ is successfully obtained after systematic optimization of growth parameters. The coverage reaches across 2 cm × 1 cm wafers and the grain size reaches 30 μm. The Raman, PL and AFM results confirmed that it is indeed monolayer. Transistors, Hall-bars and TLM structures were fabricated on monolayer WSe₂ and characterized at various temperatures. The WSe₂ transistors show clear p-channel characteristics, indicating that as-grown WSe₂ is naturally p-doped. We found that the hole mobility extracted from four-point resistance is much higher than that extracted from two-point resistance, indicating that contact resistance plays a significant role in the transistor transport. The temperature dependence of the carrier mobility extracted from four-point resistance is very weak, which may be attributed to the short-range scattering.

We also investigated the synthesis of MoS₂ by CVD and MOCVD method. We have successfully grown MoS₂ using gas phase precursor H₂S and molybdenum hexacarbonyl for the first time. This new method can potentially enable wafer-scale growth of TMDCs.

These findings will serve as a foundation for the future research and development of nanoscale electronic and photonic devices based on TMDCs, which have a wide range of applications in energy-efficient electronics, implantable medical devices, and high-speed communications.

References

- [1] Metal organic vapor phase epitaxy, webpage. Available at: https://en.wikipedia.org/wiki/Metalorganic_vapour_phase_epitaxy.
- [2] K. Kang, S. Xie, L. Huang, Y. Han, P. Y. Huang, K. F. Mak, C.-J. Kim, D. Muller, and J. Park, “High-mobility three-atom-thick semiconducting films with wafer-scale homogeneity,” *Nature*, vol. 520, no. 7549, pp. 656–660, 2015.
- [3] Y. Zhan, Z. Liu, S. Najmaei, P. M. Ajayan, and J. Lou, “Large-area vapor-phase growth and characterization of MoS₂ atomic layers on a SiO₂ substrate,” *Small*, vol. 8, no. 7, pp. 966–971, 2012.
- [4] S. Najmaei, Z. Liu, W. Zhou, X. Zou, G. Shi, S. Lei, B. I. Yakobson, J.-C. Idrobo, P. M. Ajayan, and J. Lou, “Vapour phase growth and grain boundary structure of molybdenum disulphide atomic layers,” *Nature Materials*, vol. 12, no. 8, pp. 754–759, Sep. 2013.
- [5] A. M. V. D. Zande, P. Y. Huang, D. A. Chenet, T. C. Berkelbach, Y. You, G.-H. Lee, T. F. Heinz, D. R. Reichman, D. A. Muller, and J. C. Hone, “Grains and grain boundaries in highly crystalline monolayer molybdenum disulphide,” *Nature Materials*, vol. 12, no. 6, pp. 554–561, May 2013.
- [6] X. Ling, Y.-H. Lee, Y. Lin, W. Fang, L. Yu, M. S. Dresselhaus, and J. Kong, “Role of the seeding promoter in MoS₂ growth by chemical vapor deposition,” *Nano Letters*, vol. 14, no. 2, pp. 464–472, Dec. 2014.
- [7] B. Liu, M. Fathi, L. Chen, A. Abbas, Y. Ma, and C. Zhou, “Chemical vapor deposition growth of monolayer WSe₂ with tunable device characteristics and growth mechanism study,” *ACS Nano*, vol. 9, no. 6, pp. 6119–6127, 2015.
- [8] A. Castellanos-Gomez, E. Navarro-Moratalla, G. Mokry, J. Quereda, E. Pinilla-Cienfuegos, N. Agraït, Herre S. J. Van Der Zant, E. Coronado, G. A. Steele, and G. Rubio-Bollinger, “Fast and reliable identification of atomically thin layers of TaSe₂ crystals,” *Nano Research*, vol. 6, no. 3, pp. 191–199, Feb. 2013.
- [9] A. Molina-Sánchez and L. Wirtz, “Phonons in single-layer and few-layer MoS₂ and WS₂,” *Physical Review B*, vol. 84, no. 15, Nov. 2011.
- [10] J. Aizenberg, J. B. Andrew and M.W. George, “Control of crystal nucleation by patterned self-assembled monolayers,” *Nature*, vol. 398, no. 6727, pp. 495–498, Jan. 1999.
- [11] J.-K. Huang, J. Pu, C.-L. Hsu, M.-H. Chiu, Z.-Y. Juang, Y.-H. Chang, W.-H. Chang, Y. Iwasa, T. Takenobu, and L.-J. Li, “Large-area synthesis of highly crystalline WSe₂ monolayers and device applications,” *ACS Nano*, vol. 8, no. 1, pp. 923–930, 2014.

- [12] L. Chen, B. Liu, A. N. Abbas, Y. Ma, X. Fang, Y. Liu, and C. Zhou, “Screw-dislocation-driven growth of two-dimensional few-layer and pyramid-like WSe₂ by sulfur-assisted chemical vapor deposition,” *ACS Nano*, vol. 8, no. 11, pp. 11543–11551, 2014.
- [13] T. Tsirlina, Y. Feldman, M. Homyonfer, J. Sloan, J. L. Hutchison, and R. Tenne, “Synthesis and characterization of inorganic fullerene-like WSe₂ material,” *Fullerene Science and Technology*, vol. 6, no. 1, pp. 157–165, 1998.
- [14] H. Li, G. Lu, Y. Wang, Z. Yin, C. Cong, Q. He, L. Wang, F. Ding, T. Yu, and H. Zhang, “Mechanical exfoliation and characterization of single- and few-layer nanosheets of WSe₂, TaS₂, and TaSe₂,” *Small*, vol. 9, no. 11, pp. 1974–1981, 2012.

Appendix: Optimized MoS₂ by CVD Operation Procedure



Figure 23 MTI furnace and experiment setup

(1) Substrate preparation:

Piranha cleaning is critical to ensure monolayer deposition, and not the deposition of multilayer or other undesirable allotropes. Also, a hydrophobic surface will also enhance the efficiency of transferring material in the future in. Therefore, the wafer cleaning procedure as follows:

1. Standard degrease substrate with acetone and IPA, repeat three times.
2. Soak degreased substrate in a 1:4 hydrogen peroxide/sulfuric acid solution (acid piranha) at room temperature.
3. Then turn on the hot plate and set it to 88 °C. Use two wipes to cover the hot plate. It will facilitate the uniform heat up of the substrate.
4. Put piranha cleaned substrate onto hot plate and pre-bake for 5 min.
5. Then use pipet to apply two droplets of PTAS solution to the substrate. Note: the PTAS droplet will naturally cover only part of the substrate; manually tilting the substrate will let the

PTAS cover the entire wafer. The covered solution will slowly shrink from edge to center and make a uniform coat of PTAS (if too fast, then decrease the hot plate temperature).

(2) Precursor preparation:

1. Use digital scaler (can be found in Film Stress/RTP lab in the cleanroom) to weight 50 mg of MoO_3 powder and 300 mg of sulfur powder.
2. Place measured precursor into two separate quartz crucibles, with the wafer facing down and lying in the lower level of customized sample holder or directly facing down on the ceramic boat. The sulfur crucible is placed 20 cm from the center of the first zone, where the MoO_3 crucible is placed in the second zone just the same as the placement in Figure 23.

(3) Growth Setup:

1. The growth is conducted in 15-20 sccm Ar flow after purging for 30 min at 450 sccm Ar flow. Note, it is recommended to turn on the furnace when the readout from the pressure gauge is below 40 Torr, which will be reached after roughly 30-40 min with high flow rate of Ar. The purging of furnace tube with Ar is very important to the monolayer deposition.
2. The temperature is ramped as follows: Initially, ramp up the first and second zones to 110 °C in 10 min and hold for 10 min to remove the humidity in the tube. Next, ramp the middle zone to 730 °C in 40 min. After a delay of 32 min, the left zone (containing the sulfur crucible) is ramped up to 200 °C in 8 min. This is necessary to avoid the sulfur evaporating too early, before the MoO_3 has started to vaporize. Both the first and second zones hold for 5 min.